12-2015

OPTIMIZATION OF TITANIUM LIQUID/GAS DIFFUSION LAYERS IN PROTON EXCHANGE MEMBRANE ELECTROLYZER CELLS

Stuart McCoy Steen
University of Tennessee - Knoxville, ssteen1@vols.utk.edu

To the Graduate Council:

I am submitting herewith a thesis written by Stuart McCoy Steen entitled "OPTIMIZATION OF TITANIUM LIQUID/GAS DIFFUSION LAYERS IN PROTON EXCHANGE MEMBRANE ELECTROLYZER CELLS." I have examined the final electronic copy of this thesis for form and content and recommend that it be accepted in partial fulfillment of the requirements for the degree of Master of Science, with a major in Aerospace Engineering.

Feng Y. Zhang, Major Professor

We have read this thesis and recommend its acceptance:

Matthew M. Mench. Reza Abedi

Accepted for the Council:
Carolyn R. Hodges

Vice Provost and Dean of the Graduate School

(Original signatures are on file with official student records.)

OPTIMIZATION OF TITANIUM LIQUID/GAS DIFFUSION LAYERS IN PROTON EXCHANGE MEMBRANE ELECTROLYZER CELLS

A Thesis Presented for the
Master of Science
Degree
The University of Tennessee, Knoxville

Stuart McCoy Steen, III
December 2015

ACKNOWLEDGEMENTS

I would like to thank Dr. Feng-Yuan Zhang for his guidance and support and for pushing me to work hard in my pursuit of research. I also would like to thank the other members of my committee, Dr. Reza Abedi and Dr. Matthew Mench, for their time and insightful comments.

Thanks to my lab mates, Jingke Mo, Dr. Bo Han, Zhenye (Allen) Zheng, Bo Barnhill, Aaron Liu, and Matthew Middletown for their help in lab at all hours of the day. Special thanks to Kate Lansford, Dr. Lino Costa, Doug Warnberg, and Alex Terekhov of the Center for Laser Applications (CLA) at UTSI for their help. Their assistance and wisdom are greatly appreciated. I would also like to thank Dr. Scott Retterer, Dr. David Cullen, and Bernadeta Srijanto for all their help at ORNL.

Finally, I would like to thank my friends and family for supporting me throughout school, supporting my dreams and helping me push myself towards realizing them.

This research was funded by the U.S. Department of Energy under Grant DE-FE0011585.

ABSTRACT

Polymer electrolyte membrane electrolyzer cells (PEMECs), which are reverse PEM fuel cells (PEMFCs), are effective energy storage medium by producing hydrogen/oxygen from water using electricity from renewable energy sources. This is due in part because of its efficiency, high energy density, compact design, and large capacity. In a PEMEC, a liquid/gas diffusion layer (LGDL) is located between the catalyst layer and the current distributing flow field. The LGDL is expected to transport electrons, heat, and reactants/products to and from the catalyst layer with minimum voltage, current, thermal, interfacial, and fluidic losses. Carbon materials (carbon paper or carbon cloth), typically used in PEMFCs, are unsuitable in the anode of PEMECs due to the high ohmic potential and highly oxidative environment of the oxygen electrode. The carbon corrosion and consumption will result in poor interfacial contacts that will degrade performance and efficiency. Advanced and multifunctional LGDLs with desired properties and high durability in corrosive environments are critical for improving efficiency and performance in electrochemical devices. This thesis highlights recent efforts to optimize anode LGDL properties for high-efficiency PEMECs.

By controlling the parameters of the LGDLs, a greater understanding of the physical interactions and multi-scale interfacial effects that occur in the anode is reached. The main objectives of this thesis are as follows: (1) *In-situ* investigations of the effect of previous objectives on the performance and efficiency of a PEMEC, and provide extensive analysis on testing results; (2) analysis of the corrosion that can occur in the anode during electrolysis operation; (3) development of a standard set of procedures and metrics for designing and fabricating metallic thin film LGDLs.

In this work, a set of metallic LGDLs having different thicknesses and porosities are designed and examined. It is found that the performance of the PEMEC will decrease along with an increase of LGDL thickness, but increase with a decrease of pore size. The porosity of the titanium LGDLs has less impact on PEMEC performance than in PEMFCs. The ohmic resistance plays a dominant role in electrolyzer performance, and improved performance can be obtained even at a lower porosity by reducing ohmic losses.

TABLE OF CONTENTS

LIST OF TABLES

LIST OF FIGURES

CHAPTER I
INTRODUCTION

This chapter introduces proton exchange membrane electrolyzer cells (PEMECs), specifically the liquid/gas diffusion layer component in the oxygen (anode) electrode of the cell. The motivation, research needs, and objectives will be discussed in detail.

1.1 Introduction to Proton Exchange Membrane Electrolyzer Cells

Clean and renewable energy sources are becoming increasingly prevalent due to climate change and environmental concerns over traditional energy sources. Hydrogen is a proven source of clean energy, which is currently undergoing rapid advancement. A PEMEC, which takes the reverse process of a PEM fuel cell (PEMFC), has been an effective energy storage medium by producing both hydrogen and oxygen from water. It has become more attractive due to its distinguished efficiency, high energy density, compact design, large capacity, and ability to use electricity from other renewable energy sources [1-3]. PEMECs are robust and may be used in tandem with PEMFCs in order to create highly efficient regenerative energy systems.

A PEMEC consists mainly of a catalyst-coated membrane (CCM) sandwiched by two electrodes [4]. At the anode, water is circulated through a flow field to the membrane electrode assembly (MEA) where it electrochemically reacts, and is split into oxygen and protons. The protons are transported to the cathode through the membrane, normally composed of Nafion, a perfluorosulfonic acid/PTFE copolymer. At the cathode of the cell, protons react with electrons from an external electrical source and form hydrogen gas. This gas is transported out of the cathode via a flow channel. Meanwhile, the oxygen is transported along with excess water out of the anode. The stoichiometric equations for the reaction are below.

Anode: $2H_2O \rightarrow 4H^+ + O_2 + 4e^-$

Cathode: $4H^+ + 4e^- \rightarrow 2H_2$

Global: $2H_2O \rightarrow 2H_2 + O_2$

A general schematic of a PEMEC is shown below in Figure 1. In the PEMEC, a liquid/gas diffusion layer (LGDL) is located between the catalyst layer and current collecting layer with flow field. The purpose of the LGDL is to transport electrons, heat, and reactants/products to and from the catalyst layer with minimal current, thermal, and fluidic losses [5-12]. To meet these requirements, the LGDL has to provide: (1) Simultaneous reactant/product permeability: reactant water access effectively from flow channels to catalyst layers, and products of H_2/O_2 from catalyst-layer area to flow channels, respectively; (2) Electronic and thermal conductivities: allow electrons to all reaction sites and efficient heat transport and uniform heat distribution; (3) Interfacial and mechanical effects: provide high corrosion resistance and excellent contacts with the adjacent materials/parts (BP/CD and CL), and maintain small pressure drops in the flow channel.

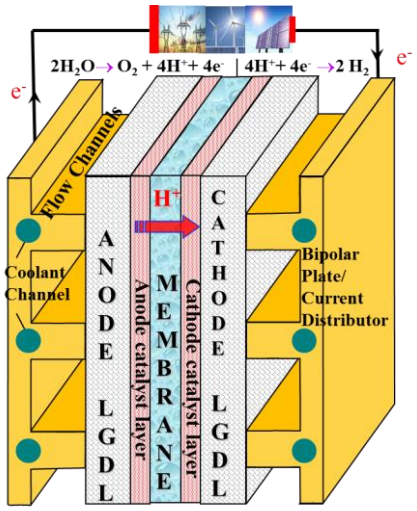

Figure 1: General schematic of PEMEC

Carbon based materials (graphite bipolar plates, carbon paper, and carbon cloth), typically used in PEMFCs [13], are unsuitable in the anode of PEMECs due to the high anodic potential that occurs during electrolysis operation [14]. This creates a highly oxidative environment, which corrodes the carbon and results in poor interfacial contacts, which will decrease the efficiency of the cell. In order to resolve this issue, materials with a high corrosion resistance must be used [15-

17]. Titanium has received considerable attention as a highly promising material for a PEM electrolyzer due to its high corrosion resistance at high positive overpotential, even in highly acidic and humid conditions. In addition, titanium provides high thermal/electrical conductivities and excellent mechanical properties.

1.1.1 Importance & Motivation (Intellectual Merit)

This research contributes to the growing knowledge of PEMEC LGDLs and aids in creating a standard of metrics for their parameters and optimal performance. The research builds upon previous knowledge and methods for fabricating metallic LGDLs, and improves upon existing designs, providing novel and cost efficient methods for fabricating metallic LGDLs for use in PEMECs and universal regenerative fuel cells (URFCs). The fabrication processes and conditions of thin titanium films with micro features is developed and optimized, and the relationship between the etching rate of titanium with micro-scale mask sizes, and etchant concentrations is investigated. Further, this research provides LGDLs with precise control of pore size, pore shape, pore distribution, and therefore porosity and permeability. It will be useful in developing the modeling and validation of PEMECs with optimal and repeatable performance.

The results of this research will impact future approaches to LGDL structure in PEMECs and URFCs, improve the efficiency of PEMECs, and aid in understanding the effects of LGDL parameters on a global system scale.

1.2 Thesis Objectives

There is a demonstrated need for additional investigations into titanium LGDL development and the use of different methods to achieve a highly controlled structure. There is also a need for understanding ways in which the LGDL structure affects the performance and efficiency of a PEMEC. The objectives described below have been determined based on these research needs.

1. Develop a standard procedure and set of metrics for the design and fabrication of titanium thin film LGDLs.

2. Study the effect of previous objectives on the performance and efficiency of a PEMEC through *in-situ* and *ex-situ* testing, and provide extensive analysis on results obtained in this manner.
3. Investigate the corrosion mechanisms that occur in the oxygen electrode.

1.2.1 Research Needs

Based on the current state of knowledge on the anode LGDL in PEMECs that has been reviewed, there is a gap in the experimental research related to the structure of LGDLs and current engineering methods to fabricate optimal LGDLs. There are several challenges still faced in improving the anode LGDL and improving the efficiency of PEMECs. These challenges are highlighted below.

Maximize control over structural parameters of LGDLs. Current methods of metallic LGDLs do not allow full control of pore shape or size. While prior research has concluded that the pore size plays important roles in the performance of PEMECs, current LGDL fabrication methods only allow for control of fiber size and overall porosity. Due to the non-ordered and sponge-like structure of sintered fiber felt, the actual pore size and shape are difficult to control.

How may the photolithography process involving titanium be optimized in order to etch a highly ordered, porous structure? Currently, HF is the etchant of choice for the wet etching of titanium. However, due to the isotropic nature of wet etching, the resistance of titanium to etching, and the hazard of HF, it is difficult to create a through-plane structure with the desired properties. There has not been much research in this field on a large scale, as generally the interest in titanium is for small features that do not etch through the substrate material.

What mechanisms does corrosion in the anode of a PEMEC cell follow? There is not enough literature at the time to know how corrosion spreads through a PEMEC. A better understanding of the corrosion and degradation of materials is needed in order to better investigate the way in which corrosion spreads within a cell.

Optimize the parameters of the LGDL from the oxygen electrode. Currently, much of this literature is based off of LGDLs used in PEMFCs. While operation is similar, there are different electrochemical reactions, environments, and mechanisms at play in the oxygen electrode of a

PEMEC. A thorough understanding of the controlling parameters of the LGDL on performance is needed in order to make an accurate assessment and create an optimal set of parameters.

1.3 Organization of this Thesis

Chapter II of this thesis provides a comprehensive literature review of the subject matter, including PEMECs, LGDLs, and the microfabrication of titanium. Chapter III explains in detail the experimental set up and the methods employed in order to accurately measure the desired data. Chapter IV analyzes this data and provides the results collected from the experimental testing. Chapter V provides a summary of this thesis, along with a conclusion derived from the results along with recommendations for future research.

CHAPTER II
LITERATURE REVIEW

This chapter provides an overview of the current state of the art regarding PEMECs, LGDL design and fabrication, along with microfabrication methods for use with titanium.

2.1 State of the Art

Prior original and novel research has investigated the use of metallic LGDLs for use in PEM fuel cells and electrolyzers. Both woven and sintered fiber felt as the general structure for metallic LGDLs has been investigated. In these studies, there has been conclusive evidence as to the importance of the anode side LGDL porosity, pore size, and two phase transport within the anode side of the PEMEC, and the crucial role it plays in the overall performance of the cell [18-20].

LGDLs serve many functions in both PEM fuel cells and electrolyzers. A properly designed LGDL must meet numerous challenges. They must provide flow pathways for H_2 and O_2 from the catalyst layer to the flow channels, as well as provide reactant water access from the flow channels to the catalyst layer. They must provide electronic conductivity to the reaction site, and provide efficient heat transport and uniform heat distribution. LGDLs must provide high corrosion resistance and serve as excellent contacts with adjacent components, and maintain small pressure drops in the flow channels.

In PEMFCs, carbon-based LGDLs are typically carbon cloth or carbon paper. These diffusion media normally have a high porosity while maintaining desirable interfacial contacts with the current collector and catalyst layers. Using carbon fiber as the basis for their structure, they have high conductivity, and a small average pore size due to the fact that the carbon fibers may have diameters on the order of 5-10 μm. Previous studies have shown that the optimum pore size of the LGDL is 12-13 μm which optimizes the performance and efficiency of the electrolysis reaction [21]. In addition, in order to improve the hydrophobicity of the LGDL on the side in contact with the catalyst, a microporous layer (MPL) is employed. In order to increase the hydrophobicity of the LGDL, it is usually treated with PTFE. This assists in the two-phase transport that occurs and helps to remove water from the catalyst layer in a PEMFC [4, 22, 23].

In a PEMEC, instead of hydrogen, water is used as the "fuel" for the system. Because of this, the reaction site is at a much higher level of saturation, which is part of the reason for the highly oxidative environment. Current titanium LGDLs, as mentioned previously, may be woven mesh, metallic foams, and sintered fiber felt [24, 25]. Woven meshes are difficult to machine, and do not have the pore size desired due to limitations of the material and available methods. The felts are similar in random structure to carbon paper. Shaved fibers of metal are sintered together to form a non-ordered porous material. The fiber diameter of titanium normally may vary from 20-100 μm, which is much coarser than the carbon fiber employed in PEMFC LGDLs. It is possible still to fabricate these felts with an average pore size of 12-13 μm, but at the cost of reducing the overall porosity of the structure. While the desired porosity is 70-80% for the LGDL, using 20 μm titanium fibers with an average pore size of 12.7 μm leads to a porosity of about only 50%. Due to the limitations of fiber size, compromises must be made with titanium felt. In addition, their extra thickness increases significant electrical conductive path and fluidic resistance. Because of these compromises, there has been a renewed interest in thin film LGDLs for use in both PEMFCs and PEMECs [13, 26-28].

Currently, there are two primary methods for the etching of titanium [29]. Wet etching is cost effective, but isotropic and difficult to control [30, 31]. For titanium, HF and other derivatives such as BOE and HF with HNO_3 are used [32-35]. The aspect ratio of the features that may be achieved using these methods are typically 1:1. The etching rate may vary from 200 nm/min - 2 μm/min. Dry etching methods allow for much higher aspect ratios in the titanium, but are more time consuming and costly [36]. The metal anisotropic reactive ion with oxidation (MARIO) process is favorable, as it allows for aspect ratios over 10:1, and etches at a rate of about 0.5 μm/min [37-39]. This process is a cyclical procedure, alternating chlorine plasma etching and oxygen-induced reactive ion etching. This technology has been demonstrated capable of the bulk micromachining of titanium, and creating high aspect ratio structures such as 25 μm trenches with 85° ± 1° sidewalls and seen in Figure 2 [40, 41].

While the MARIO method is promising, it is costly and difficult to perform. An understanding of the isotropic behavior of wet etching would allow for the manipulation of mask design. This strategy was employed by Zhang in the etching of thin copper films [7]. Using a 12.5 μm film with

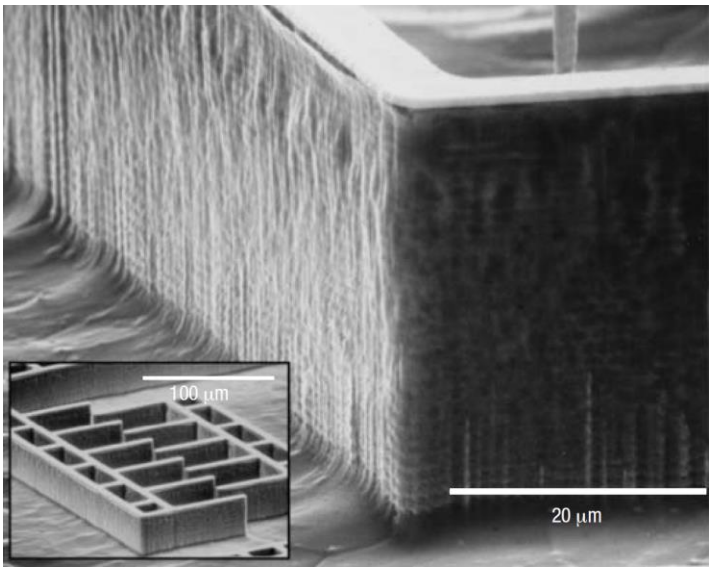

Figure 2: High aspect ratio etched titanium structure [37]

a mask feature diameter of 5 μm, they were able to etch through the film and create features that were 15-25 μm in diameter. Mask feature shape did not affect the etching profile, since the isotropic nature led to circular features after an extended etching period; however, again by manipulating mask features, complex shapes may be fabricated by reducing the spacing between mask features.

CHAPTER III
EXPERIMENTAL METHODS

This chapter presents the experimental methods and procedures used for creating the experiment, collecting data, and later processing the collected data for use in data analysis and post-processing.

3.1 Introduction

In this work, seven titanium liquid gas diffusion layers, including both titanium mesh and felt LGDLs, were designed to investigate the effects of LGDL porosity and thickness on the performance and impedance of a PEMEC based on the successful development of titanium bipolar plates for the robust testing. A stainless steel mesh LGDL is also designed in order to investigate the oxidative environment of the anode. The micro-scale characteristics of the LGDLs are detailed in Table 1, and Figure 3 shows the typical structure of the LGDL meshes. Both electropotential performance and galvanostatic electrochemical impedance spectroscopy are conducted on the different LGDLs in order to evaluate the effectiveness of altering the aforementioned parameters. Prospects for future LGDL development in PEMEC are discussed.

The research of this thesis follows both an *ex-situ* and *in-situ* experimental approach. The research concludes with experimental testing of the fabricated and modified LGDLs in a PEM electrolyzer test cell.

3.2 Ex-Situ Methods

Ex-situ methods were employed both before and after the testing of the LGDLs. They were used to characterize the physical structure of the LGDLs, and the changes that occurred to the structure during testing. Changes included physical deformation due to compression, oxidation from the environment of the anode, and consumption of titanium in an electrochemical environment.

Table 1: Titanium LGDL parameters

Subgroup	Sample	Thickness (µm)	Porosity
A	A1	534	0.64
	A2	278	0.64
	A3	170	0.64
B	B1	204	0.77
	B2	204	0.62
	B3	204	0.27
Felt	F1	500	0.73
SS	SS	100	0.36

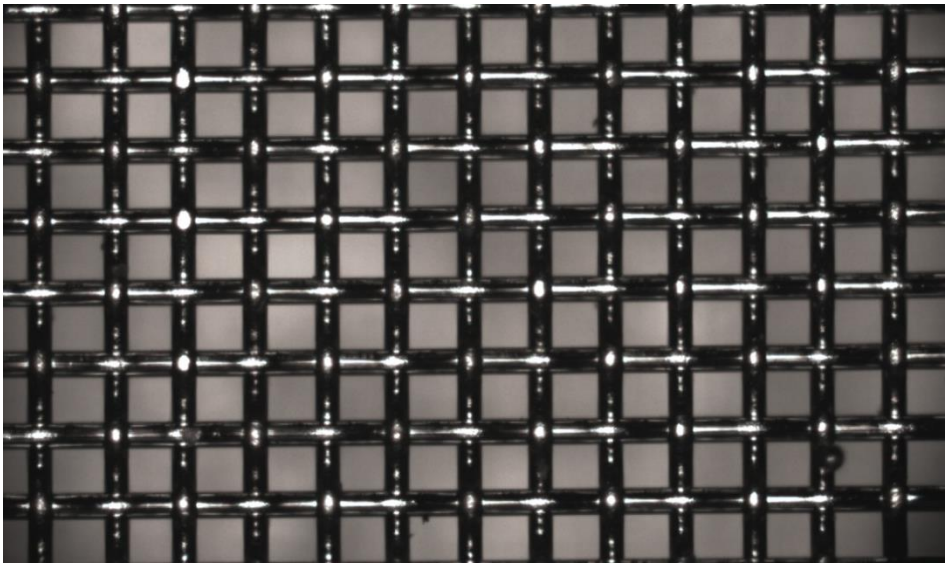

Figure 3: Typical LGDL mesh

The morphological characteristics of the liquid/gas diffusion layers and catalyst-coated membranes used in testing were observed using a field emission scanning electron microscope (SEM). The SEM used was a JEOL JSM-6320F with an accelerating voltage of 0.5-30kV, a magnification range of 130x ~ 650,000x, and a 5-axis specimen mount. The working distance used ranged from 25mm to 6mm. Images were captured, processed, and analyzed by TEAM software. Figure 4 shows SEM images of three different LGDLs and their topological features. Both SEM and energy dispersive x-ray spectroscopy (EDS) were used as the main sources of ex-situ investigation. SEM allows for high resolution analysis of the morphological characteristics of the LGDLs as well as the catalyst layers used in the PEMEC during testing. EDS allows for the identification of any impurities, contaminants, and oxides that may form on the LGDLs during testing.

Figure 4: SEM of LGDLs (left: Toray-090 CP; center: Titanium mesh; right: Titanium felt)

3.3 In-Situ Testing

In order to observe the effectiveness of the thin film LGDLs on PEMEC performance and efficiency, electrochemical testing of the cell must be employed. For this, a single PEMEC was designed and fabricated for the experiments conducted. The cell consisted of two endplates made from commercial grade aluminum that were designed to provide an even compression to the cell. In order to apply an electrical current to the reaction site, a copper plate was inserted at the cathode as a current distributor. The cathode flow field was fabricated from graphite and used a parallel

flow field to help remove produced hydrogen gas from the reaction site. In a PEMEC stack, this component would serve as the bipolar plate as well, but for experimental purposes our PEM electrolyzer consisted of only one cell. The anode current collector/flow field was fabricated from grade 2 titanium and used a parallel flow field to evenly distribute DI water over the active area of the LGDL and cell. In order to prevent leakage, gaskets were fashioned from PVC around the LGDLs that were fabricated. For the experiments the cell was compressed by eight evenly distributed bolts, which were tightened to 40 lb.-in. of torque during cell assembly using a standard torque wrench. The CCM consisted of a Nafion membrane sandwiched by catalyst layers, and had an active area of 5 cm^2.

In the electrolyzer test, Toray-090 carbon paper treated with 5% PTFE was used as the cathode gas diffusion layer. At the anode, both titanium meshes and felt were tested for investigating the effects of LGDL thickness and pore morphology. The Toray 090 carbon paper has a thickness of 280 µm and a porosity of 0.78. The titanium and stainless steel mesh LGDLs were comprised of an array of metal fibers, and the mesh fiber diameter is approximately half of the thickness of each GDL. As seen in table 1, Subgroup A has the same porosity with varying thickness, and Subgroup B has the same thickness with varying porosity. The felt used in testing had a large thickness of 500 µm and porosity of 0.73. It had no surface treatment, and the fibers had a diameter of about 20 µm, as shown before in Figure 3.

The catalyst-coated membrane is comprised of Nafion 115, a perfluorosulfonic polymer with a thickness of 125 µm, an anode catalyst layer with an IrRuOx catalyst loading of 3 mg/cm^2, and a cathode layer with a Platinum Black (PtB) catalyst loading of 3 mg/cm2. SEM images of the catalyst layers may be seen in Figure 4. Both images are taken at a magnification of 50,000X. Both catalyst layers are porous and have a homogeneous composition. The IrRuOx layer clumps together, giving it a paste-like appearance, while the PtB has a smoother composition than the IrRuOx.

The LGDLs in Subgroup A all had the same porosity with varying thickness, so the results obtained from their testing investigate the direct effects of LGDL thickness on the performance of the cell. As can be seen in Figure 5, the needed operating voltages for all three samples are increased with the current density, j, which is directly related to the hydrogen production, n_{H_2}, as defined below:

$$n_{H_2} = \frac{j}{2F} \quad (1)$$

Where F is Faraday's constant. Generally, the total operating voltage includes open circuit voltage (OCV), activation overpotential, and polarizations due to transport and ohmic losses. Higher current densities mainly result in larger polarizations, thus leading to higher total operating voltages and lower performance of the electrolyzers.

In order to test the LGDLs in the PEMEC, the cell was attached to an electrolyzer control system that allowed for performing chronopotienometry (CP), impedance spectroscopy, and durability testing of the cell. CP measured the output voltage of the cell given an input current density. This data assisted in creating polarization curves of each cell with different LGDLs, as shown in Figure 6. This data was then compared directly between different LGDLs.

Galvanostatic electrochemical impedance spectroscopy (GEIS) was used for evaluating the impedance of the PEMEC. This method, which applies an input current density over a frequency spectrum, is less conventional than potentiostatic impedance spectroscopy (PEIS), but is more appropriate for electrolyzers, since they are in a constant charging state. While a complex subject, the impedance in PEMECs mainly consists of ohmic, activation, charge-transfer, and mass-transfer impedance, which all result in performance losses of the PEMEC.

For the *in-situ* investigation performed, a test system that consisted of an electrolyzer test stand, EIS, a flow control and measurement system, and a hydrogen evacuation setup was used. The cell was attached to the control system with a current range up to 100A and a voltage range up to 5V. The hardware was connected and used in tandem with Bio-Logic's EC-Lab software. This was used to conduct performance and efficiency testing, as well as EIS. For the flow control, a system of plastic tubing was connected to the PEMEC. While the cathode piping was for the safe exhaustion of hydrogen gas that formed during electrolysis, the anode piping used a diaphragm liquid pump from KNF Neuberger to circulate deionized (DI) water at a constant volumetric rate of 40 ml/min through the anode. A general schematic of the test system is shown in Figure 5, and the composition of the PEMEC is shown in Figure 6. The PEMEC operated at room temperature.

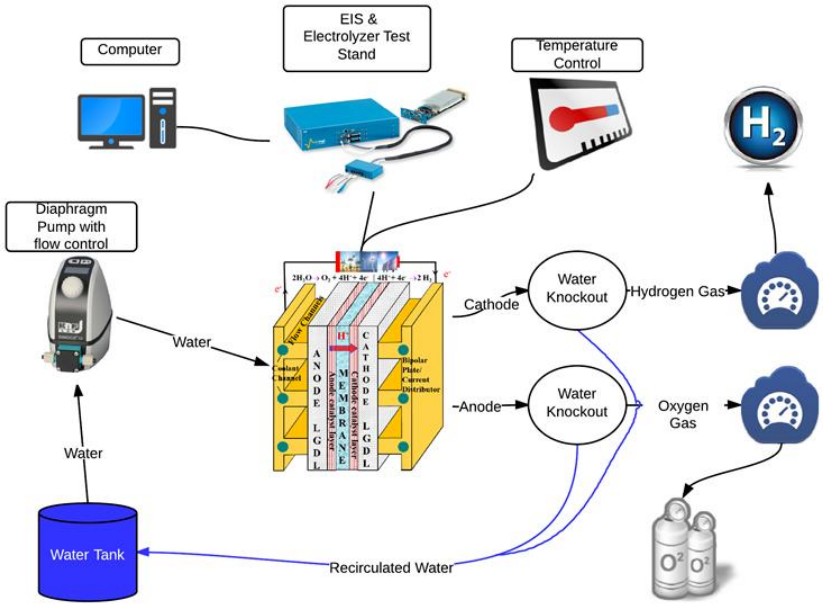

Figure 5: PEMEC test system

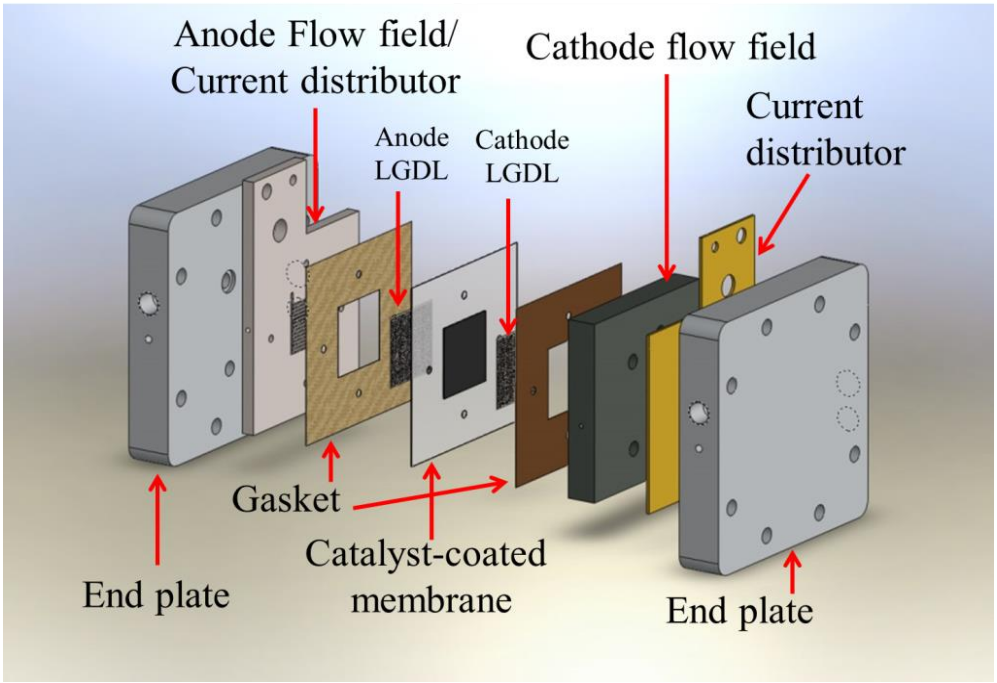

Figure 6: Components of PEMEC

3.3.1 Chronopotentiometry

For the performance testing, a current was applied to the PEMEC over a constant period of time. The current increased in steps from a current density of 0.0 A/cm^2 to 2.0 A/cm^2 in increments of 0.2 A/cm^2. At each current density the potential of the cell was measured for five minutes before incrementing the current density again. Five minutes was chosen as an acceptable amount of time at each current density as it was empirically observed that the cell was relatively stable at for those lengths of time and any extended length of time was superfluous.

3.3.2 Electrochemical Impedance Spectroscopy

There are two powerful methods of analysis that may be used to investigate the performance and degradation that may occur to a PEMEC. They are EIS and energy dispersive x-ray spectroscopy (EDS). Both of these methods were employed in order to perform in-situ and ex-situ analysis on a PEMEC developed in lab.

GEIS was used for evaluating the impedance of the PEMEC. The equipment used had an operating current of -100A – +100A and a voltage of 0.6V – 5V. The current precision was 100 fA. Impedance was measured at 0.4, 0.8, 1.2, 1.6, and 2.0 A/cm^2. The scanning frequency went from 10 kHz to 5 mHz, and recorded six points of data per decade.

For the *in-situ* testing, GEIS was desirable because it is a macroscopic electrochemical technique that may be used while the cell is performing electrolysis. It is the most useful for studying the electrode-electrolyte interface as well as analyzing corrosion that may occur in a PEMEC. From performing GEIS, the ohmic, activation, and transport resistances in a PEMEC may be determined. In a typical GEIS test a frequency range from 10 kHz – 5 mHz is performed, with the current applied to the cell remaining constant. The ohmic resistance typically dominates the losses in performance for the PEMECs of interest. The activation impedance can be derived from the slope of the arc in the Nyquist Plot in the middle of frequency range, and the transport resistance may be found from the difference between the values of the x-axis intercepts at the low frequency range. Figure 7 below shows an example of data that may normally be obtained from GEIS analysis, plotted in the complex plane.

In the figure, the real and imaginary axes are normalized by multiplying the values measured by the active area of the cell. There is one more step of normalization, where the real axis values

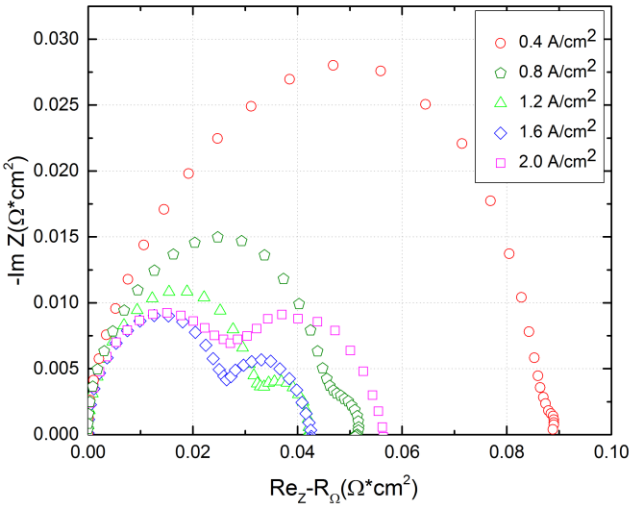

Figure 7: Nyquist plot showing the same LGDL in a PEMEC measured under different operating conditions

are further normalized by subtracting each value by the ohmic resistance. In a Nyquist plot, the ohmic resistance is the value of the leftmost x-axis intercept at high frequency. Transport resistance is calculated by taking the difference between both x-axis intercepts for a given arc, and the activation impedance is described qualitatively by the slope of the arcs in a Nyquist plot.

GEIS allows for conclusions regarding the nature of the LGDL in the anode of a PEMEC to be reached. As the interfacial contact increases and the thickness of the LGDL decreases, the ohmic impedance greatly decreases. From other GEIS analysis performed during testing it is shown that even though some GDLs may have a low porosity (<40%), their favorable interfacial contact leads to a low ohmic resistance and thus a higher performance.

Figure 6 shows that the transport resistance in a PEMEC varies depending on the current density the cell is run at. The transport resistance is denoted as the rightmost x-axis intercept in low frequency range. The reason for the change in transport resistance at different current density is because there is a greater liquid water consumption and the difference in H_2/O_2 production between each current density.

3.4 Titanium Microfabrication

In order to fabricate LGDLs from titanium thin film, a deep understanding of the fundamentals of photolithography is needed. In order to control the etching, several photomasks must be designed and made with different features, including pore size and shapes [8]. The photomasks contain an array of pores that allow for the fabrication of an LGDL that is the size of the active area of the test PEMEC, or about 5 cm^2.

Layout Editor, or L-Edit, from Tanner EDA was used for photomask design. This software allows for submicron mask design and the creation of mask features infrastructure, which may be used to easily modify and vary the mask pattern. Once an appropriate mask was designed, the photomask was fabricated at the Center for Nanophase Material Sciences (CNMS), located at Oak Ridge National Laboratory (ORNL). This is the result of a research relationship with CNMS. An example photomask layout design is shown in Figure 8 below. In this design, the spacing between each feature is 200 μm, and the diameter of the features increases from 5 μm to 25 μm with different shapes, including circles, triangles and squares.

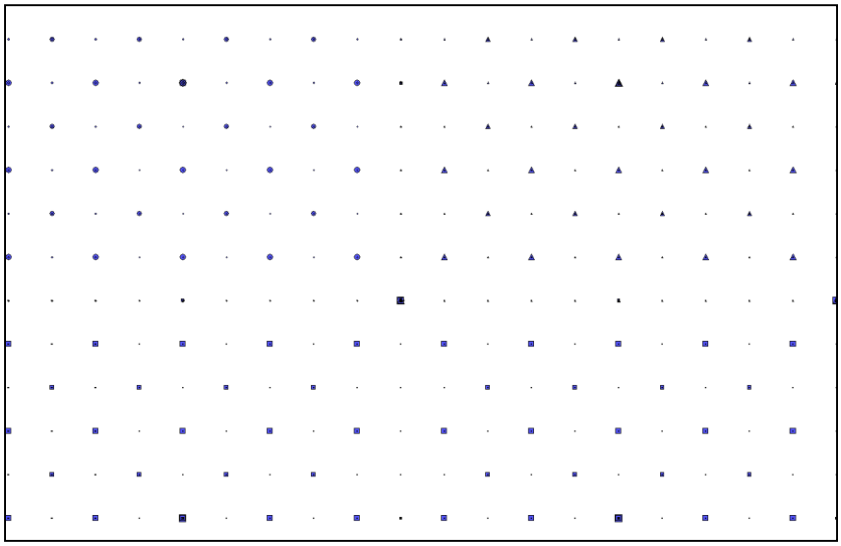

Figure 8: Photomask design. Feature size range from 5-25 µm and spacing is 200 µm

There are two different film thicknesses used in the etching: 25 μm and 10 μm. This initial photomask will contain an ordered array of pore features ranging in diameter from 5 μm to 25 μm. There will be 200 μm between each feature in order to allow enough space while etching the features. There will be three different basic pore shapes on the mask in order to investigate the effect of feature shape on the etching on titanium: square, triangle, and circle pores. This array will cover an area of $5cm^2$. Along the perimeter of this array, there will be ordered rows of the three basic pore shapes increasing in diameter from 3 μm to 98 μm in increments of 5 μm, and from 5 μm to 100 μm with the same increment. There will be 500 μm between each of these features, and will be used to examine the effect of pore size on the etching of the titanium film.

Once fabricated, a procedure for preparing the titanium film samples was detailed. Figure 9 shows the general procedure that will be employed. This procedure includes the following:

1. Proper cleaning of preparation of titanium film and silicon wafer
2. Mounting titanium film on to silicon wafer for structural integrity
3. Even application of photoresist to titanium film
4. Using photomask, expose photoresist layer to UV light
5. Develop photomask pattern on photoresist
6. Hard bake developed pattern

There are many different types of photoresist that may be used for patterning the titanium film. From the literature review conducted, SPR 220 was the photoresist chosen. SPR 220 has preferable selectivity to HF, which is the main etchant that will be used for wet etching the film. A photoresist layer thickness of 4.5 μm was made. In order to assist with the adhesion of the photoresist to the titanium film, P20 was used, and was applied using a spin coat method.

3.4.1 Wet Etching

Wet etching was the micromachining method investigated for LGDL fabrication. Different etchants were used in order to study their effects on the final structure of the titanium film pattern and surface. A total of three different etchants were used. The first is a buffered oxide etchant (BOE). This etchant has a lower concentration of HF, and is also mixed with NH_4F in order to

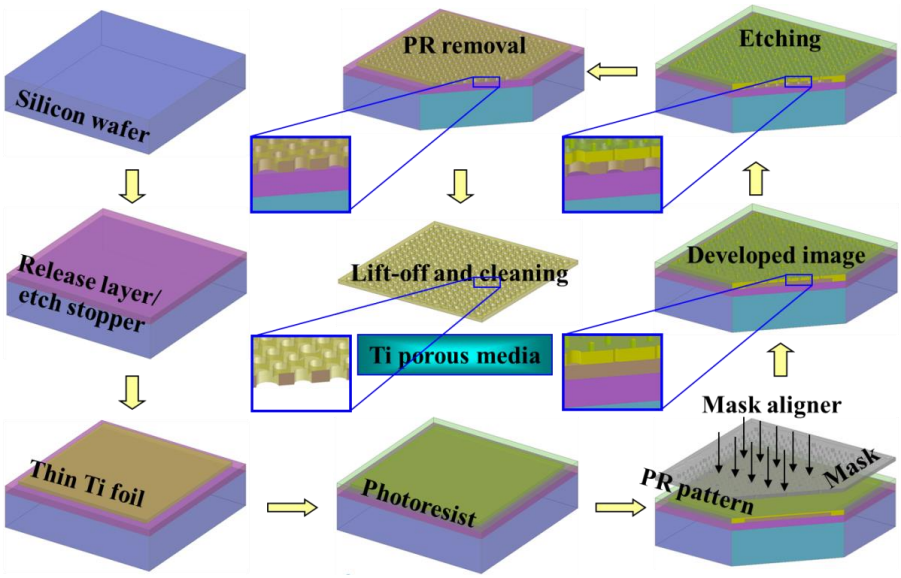

Figure 9: Fabrication procedure of porous titanium thin film

improve control over the etch process. The other etchant mixture is HF with HNO_3. This etchant also is used in cases of process control. The nitric acid in the mixture is normally only 0.7-1.2% by weight, and helps to etch away the alpha phase of the titanium crystal structure. Diluted HF will also be used for etching. In both the case of HF and HF mixed with HNO_3, two concentrations of HF will be tested: 1% and 5% by weight. The rest of the composition of the etchant mixtures will be deionized (DI) water.

Using the initial photomask described in the previous section, the etchants were tested on samples of the titanium foil to investigate their properties. The typical etch rate in μm/min of the etchants was explored. Special handling of the etchants is needed, and the etching will take place under a fume hood in case of spill.

Maintaining clean samples throughout the etching process will be of utmost importance. Impurities on the foil and on the developed photomask can affect the etching and lead to irregular features. In an effort to reduce the amount of possible impurities, the etching was conducted in a Class 1000 clean room at the Center for Laser Applications (CLA) on UTSI campus.

There are different strategies for applying the etchant to the developed foil sample. One common method that is simple but effective is the spill over method. This involves applying an even layer of the etchant over the developed area, and stirring the etchant in order to maintain an even etching rate over the entirety of the foil and remove ions from the reaction site between the foil and etchant.

Since wet etching is an isotropic process, that is, the foil will etch in-plane at the same rate through-plane, an interesting phenomenon will occur. Since the foil will be adhered to a silicon wafer using photoresist that is non-reactive to HF etchant, once the foil is etched through, the features will continue to etch in-plane. This will increase the diameter of the pores being etched. Because of this, the mask must be designed with smaller features than those desired.

CHAPTER IV
EXPERIMENTAL RESULTS & DISCUSSION

The focus of this chapter is the presentation of the case results and sample trajectory profiles to form the foundation for optimization comparison and analysis.

4.1 GEIS & Performance Testing Results

In the CP experiments per performed, there were stark differences between the SS316 mesh and the titanium mesh. As shown in Figure 10 below, while the titanium mesh had a linear and smooth polarization curve, the stainless steel mesh had a steep and irregular slope. This was the earliest indication of significant corrosion in the stainless steel mesh. The impedance results support the difference that was seen in the performance of the LGDL materials. As shown in Figure 11, the ohmic resistance, which is recorded as the point at which the Nyquist plot first intersects the x-axis, of the stainless steel mesh is more than three times that of the titanium mesh, 0.66 $\Omega \cdot cm^2$ to 0.20 $\Omega \cdot cm^2$. This difference is due to less contact resistance, better conductivity, and less oxidation degradation in the LGDL-catalyst interface, which is part of the MEA.

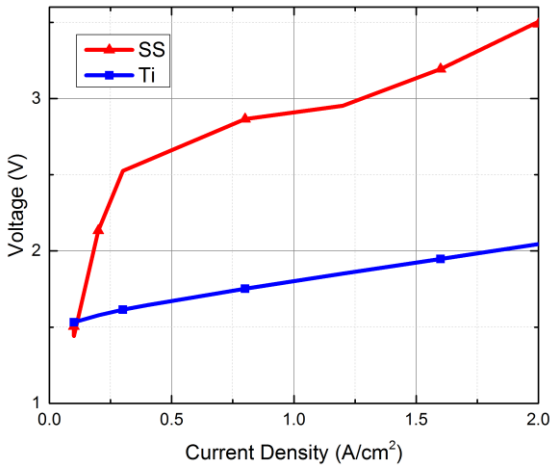

Figure 10: Performance results from testing

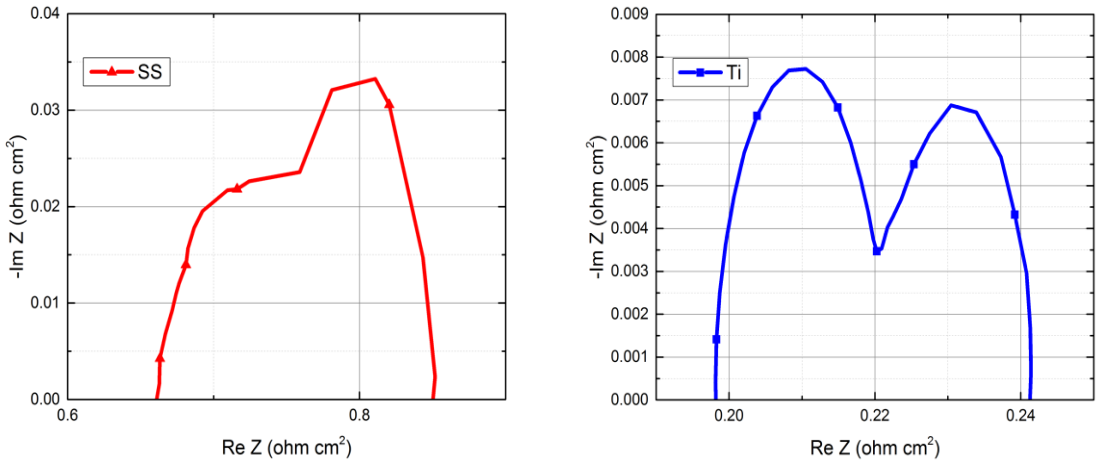

Figure 11: Impedance spectroscopy results: left: SS LGDL; right: Titanium LGDL

Figure 12 shows the relationship between the input current densities and operating voltages needed with different thicknesses of anode titanium LGDLs with the same porosity of 0.64. The PEMEC operated at room temperature for this testing. For all the samples, the operating voltages are increased with the input current densities, while exhibits different evolution rates. With the same current density range, a larger variation of operating voltages is obtained from the thicker LGDLs. At the same current density, the operating voltages are different from the test samples. For instance, at 1.2 A/cm^2, the operating voltages are increased significantly from 2.14V to 2.62V with the anode LGDL thickness increasing from 170 μm to 534 μm, respectively. The result indicates that electrolyzer performance significantly decreased as the thickness of the LGDL increased.

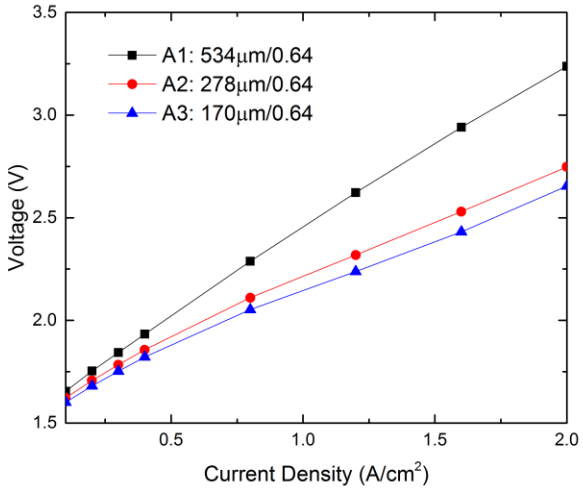

Figure 12: Electrolyzer performance with different anode LGDL thickness

For better understanding the mechanisms involved, the GEIS testing was performed in-situ with all designed samples. Over the frequency range from 10 kHz to 5 mHz, there were two depressed arcs, which clearly demonstrated three separate impedance regimes: high-frequency impedance (> 1 kHz), medium-frequency impedance (1 kHz -4 Hz), and low-frequency impedance

(< 4 Hz). The high-frequency resistance, which mainly represents total ohmic resistance, is the leftmost intercept of the depressed arcs with the real axis at the high-frequency end. It includes the ohmic resistances of all electrolyzer components, including bipolar plates, diffusion media, electrodes and membranes, and the associated interfacial resistances between them. In the medium-frequency range, the activation losses and charge-transfer resistances on both the anode and cathode dominate the overall impedance response. The low-frequency range correlates to the mass-transport resistances, which can be associated with many mechanisms, mainly phase transport losses across electrodes and diffusion media in the electrolyzer, including water/oxygen/hydrogen transport resistance, and oxygen/hydrogen bubble coverage in reaction sites [24-28]. As shown in Figure 13, the impedance spectra varies with the thickness of anode LGDLs. The ohmic resistances significantly decrease from 0.78 Ω*cm^2 with a thicker LGDL of 534 µm to 0.47 Ω*cm^2 with a thinner one of 170 µm, and the other resistances due to activation, charger transfer, and transport losses reduce from 0.38 Ω*cm^2 to 0.47 Ω*cm^2, respectively. These results indicate a thicker titanium LGDL with same porosity cause higher transport and ohmic losses, thus reducing the PEMEC performance, as shown in Figure 12.

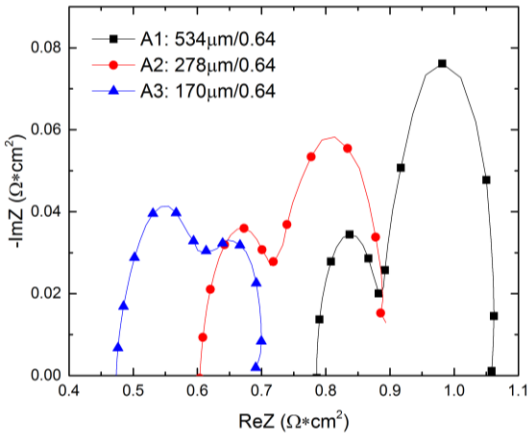

Figure 13: GEIS results with different anode LGDL thickness

With the same thickness, the effects of varying LGDL porosity was also investigated using Subgroup B. Since the LGDLs tested are titanium meshes, porosity is defined as the geometric

open area of the mesh. For example, for Sample B3, the LGDL has an open area of 27%, while the remaining 73% of the area was titanium. The performance results for Subgroup B are plotted in Figure 14. As the porosity is decreased from a porosity of 0.77 to 0.27 at a fixed LGDL thickness of 204 μm, the operating voltage needed is reduced at the entire current density range, which indicates a better performance. With the same thickness and same titanium fiber diameter in this subgroup, the decrease of the porosity needs to add more fibers to increase mesh numbers, thus leading to a smaller pore size. The pore sizes of the titanium LGDL samples B1-3 decreased from 699 μm, 391 μm and 108 μm, respectively.

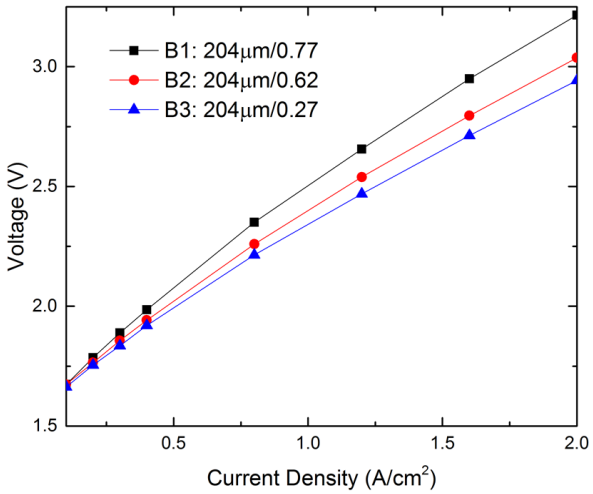

Figure 14: Electrolyzer performance with different anode LGDL porosity

Physically, lower pore sizes lead to greater contact area with the CCM and a smaller ohmic resistance as demonstrated by the GEIS. Similar to the plots in Figure 13, there are three regimes for the GEIS measurements from subgroup B. Clearly represented is the impedance in the different frequency ranges: high-frequency impedance (> 1 kHz), medium-frequency impedance (1 kHz – 4 Hz), and low-frequency impedance (< 4 Hz). As shown in Figure 15, there were few differences observed for the resistances of mass transport and activation, while the ohmic resistances were

reduced from 0.46 Ω*cm^2 to 0.37 Ω*cm^2 when the pore size was decreased from 699 µm to 108 µm, respectively. This sheds more light on the earlier performance data as shown in Figure 12. While it has a lower porosity, the B3 LGDL with a smaller pore size of 108 µm has a significantly larger surface area with which to make contact with the reaction site on the CCM, which leads to an overall lower potential and greater performance [4, 5, 10, 42-44].

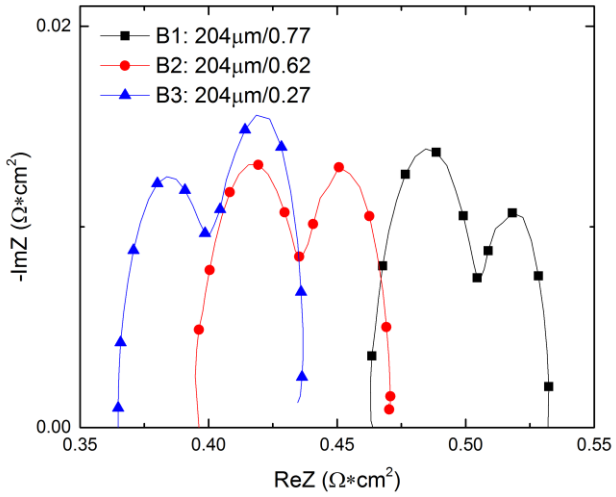

Figure 15: GEIS results with different anode LGDL porosity

To further investigate LGDL effects, a titanium felt LGDL, as shown in Figure 4, was introduced for testing. As shown in Table 1 prior, its porosity and thickness are 0.73 and 500 µm respectively, while its average pore size is about 60 µm, much smaller than other titanium LGDLs. Figure 16 shows its performance tested in the electrolyzer with a flow rate of 40 ml/min at room temperature. Similar to the other titanium LGDLs, its operating voltage is increased with current density, and it performed most similarly to sample A3. Since the felt LGDL has a smaller pore size, it is expected to provide a better interfacial contact with the catalyst layer. Although the titanium felt LGDL is much thicker than sample A3, it still maintains a lower ohmic resistance and smaller transport resistance due to a large porosity, and thus leading to improved PEMEC

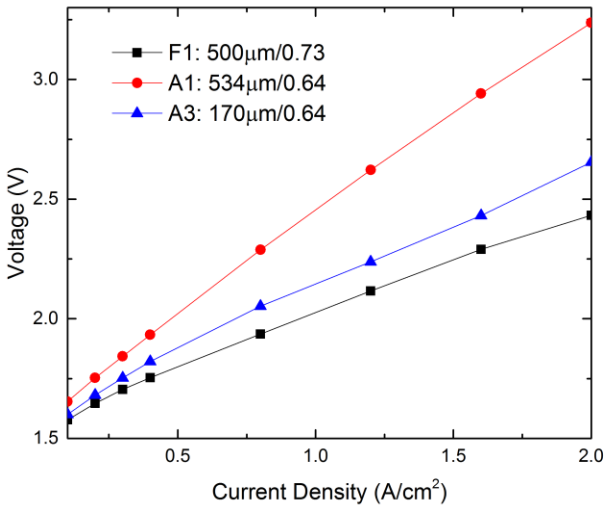

Figure 16: Performance with titanium felt LGDL

performance. These results are demonstrated in the measured GEIS as shown in Figure 17.

In addition to promoting interfacial contact, the smaller pores are preferred for more uniform thermal and electrical distributions and higher catalyst utilizations as well. In electrolyzers, the electrochemical reactions occur only on "multiphase interfaces," including electron conductors, catalysts, proton carriers, and fuels/products. For instance, water oxidation at the anode needs: (1) electrons from LGDLs and electrode current distributors, (2) liquid water from the LGDL pores, (3) catalyst from catalyst layer, (4) protons to the electrolytes in catalyst layers and PEMs, and (5) gaseous oxygen to the flow channel via LGDL pores.

The smaller pore size greatly enhances catalyst utilization and uniform thermal/electrical distribution across LGDLs and catalyst layers, and minimizes the ohmic loss in both interfaces between the LGDL and catalyst layer/flow field. Note that the applications of titanium felts in PEMEC have been limited due to their costs, manufacturing complexities, and thicknesses and/or

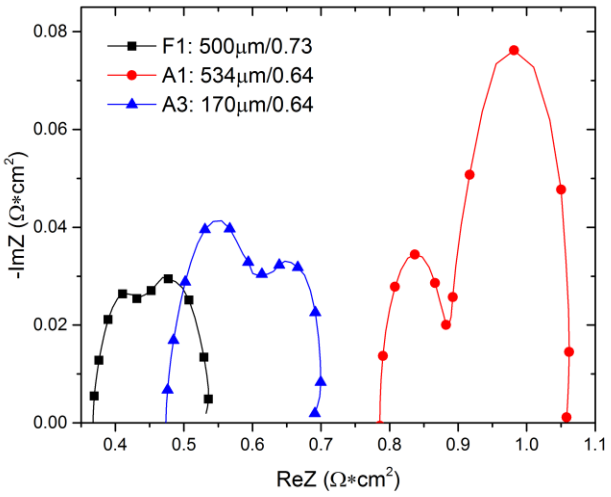

Figure 17: GEIS comparison with titanium felt LGDL

volumes. With optimal designs of thickness, porosity, and pore size, similar or even improved performance can be achieved with mesh-structured LGDLs by taking advantage of straight pores. As shown in Figures 16 and 17, a resistance reduction of LGDL A3 will make it possible to

decrease the PEMEC operating voltage and enhance its performance. In addition, precise controls of pore size, pore shape, pore distribution, and therefore porosity and permeability can be succeeded with LGDL straight-pore features based on advanced manufacturing. It can be very useful to develop modeling and to validate simulations of electrolyzers with optimal and repeatable performance. This development leads directly to reducing the cost, volume, and weight of the LGDL itself and the system as a whole.

4.2 Post Test Investigation of Corrosion

After testing of the PEMEC concluded, the cell was disassembled and further investigation of the LGDLs occurred. This can be done using SEM microscopy in tandem with EDS. The EDS detector used is from EDAX, and uses their TEAM software to perform both image processing and mapping of the sample of interest. EDS allows for viewing the physical characteristics of the materials before and after testing, and an analysis of the elements that make up the sample.
Figure 18 contains SEM images obtained in this manner, and shows before and after images of the anode and cathode LGDLs after the stainless steel mesh was tested. As shown in the images, there was a significant amount of corrosion in the stainless steel mesh. On the contrary, there is no corrosion found on the titanium mesh. What is interesting to note is that there was also evidence of iron oxide present on the carbon paper LGDL located at the cathode. This was supported by the EDS results gathered and detailed in Table 2.

Table 2 shows the atomic concentration of elements found in both the fresh and used LGDL samples. An example of the spectrum found during EDS analysis is shown in Figure 19. As mentioned above and seen in Table 2, there is a large amount of iron and oxygen found on the used carbon paper. After cell operation concluded, testing was performed on the membrane to test for any leakage, but no source was found. This leads us to believe that iron contaminants from the anode LGDL migrated through the membrane and attached to the cathode GDL. While the mechanism of this reaction is unknown, further research is planned to better understand the phenomenon.

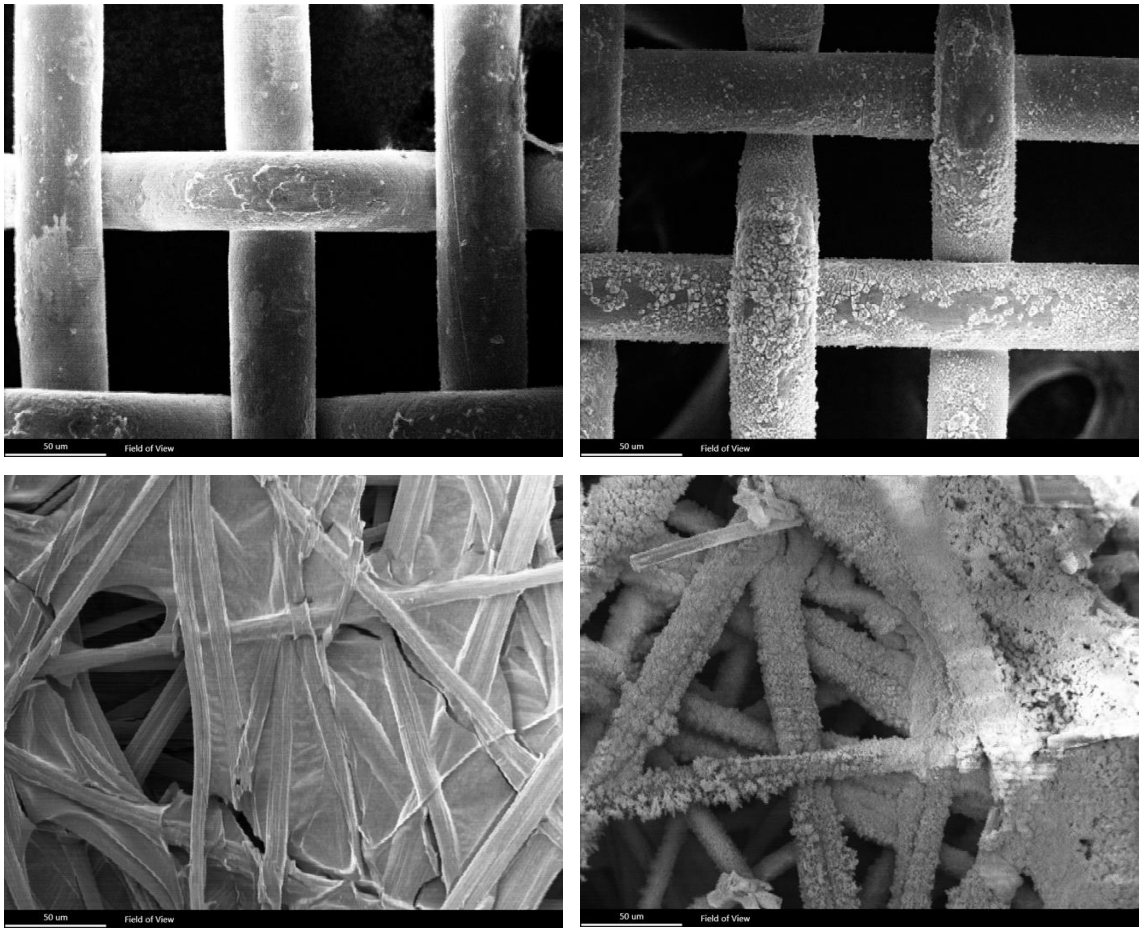

Figure 18: (left to right, top to bottom): A) Fresh SS LGDL; B) Tested SS LGDL; C) Fresh sample of carbon LGDL; D) Tested carbon LGDL; There is a significant amount of iron oxide on the carbon paper.

Table 2: Atomic concentration of elements in fresh & used LGDLs

Test Sample	Atomic Concentration					
	Iron	Carbon	Fluorine	Oxygen	Chromium	Nickel
Fresh SS	60.27	0	0	12.67	15.63	11.43
Used SS	18.21	26.28	0	47.29	5.55	2.67
Fresh CP	0	95.8	4.2	0	0	0
Used CP	28.45	19.25	.89	51.41	0	0

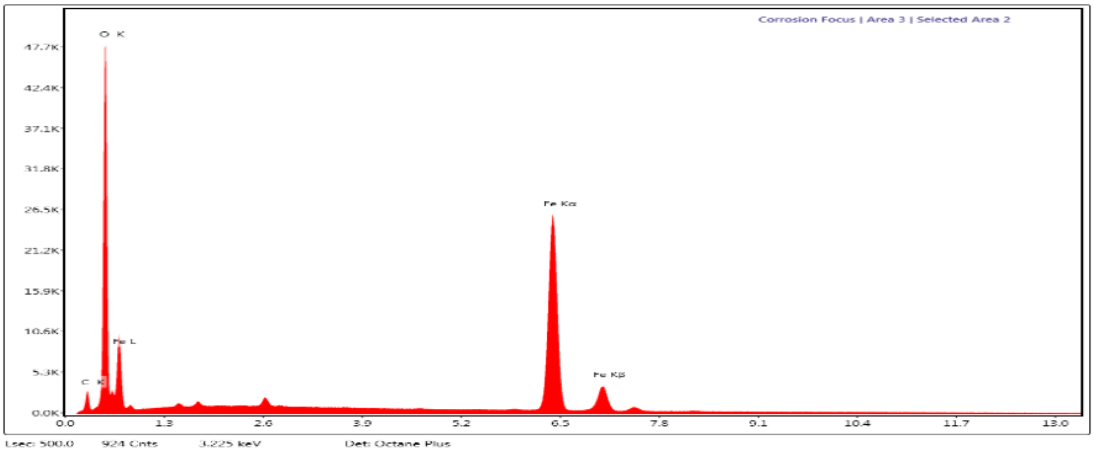

Figure 19: Example of spectrum found during EDS analysis

4.3 LGDL Microfabrication Results

Two photomasks were fabricated during this research, including the initial test photomask. Both were fabricated using e-beam lithography at CNMS. A rapid access proposal was accepted in June of 2014 that allowed for initial collaboration between NanoHelp group and CNMS. An image of the initial test mask is shown in Figure 20.

Using the photomask, the initial procedures regarding the wet etching of the titanium foil were performed. 1% and 5% HF were tested, along with BOE. SPR 220 photoresist was used, both for adhering the foil to the silicon wafer as well as for patterning the titanium foil. For

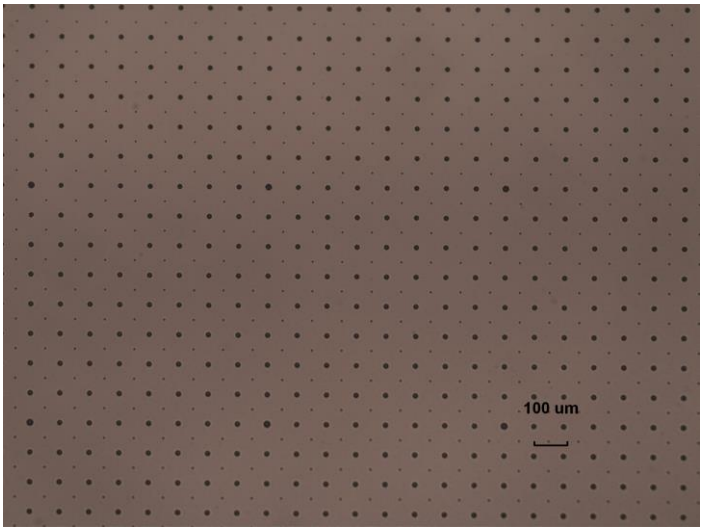

Figure 20: 10x image of the initial fabricated photomask

cleaning the titanium foil, the foil is first washed in an acetone bath in an ultrasonic agitator for 20 minutes to remove impurities, and then washed in an isopropanol bath in an ultrasonic agitator for another 20 minutes to remove any acetone residue. After both washings, the foil is dried using nitrogen gas.

In both cases, the foil is pre-etched, to serve as one last cleaning step before etching. It has been observed that BOE etches titanium at a rate of about 125 nm/min, and was used to ensure

uniformity across the surface of the foil. To pre-etch, the surface of the foil was covered in an even layer of BOE for two minutes, after which the foil was rinsed in DI water thoroughly.

At the conclusion of the hard bake, the foil may be etched. Currently, preliminary results demonstrate the following average etch rates for the following etchants shown in Table 3. Due to differences in the size of features on the mask, the etch rates will vary.

Table 3: Etch rate of etchants used in titanium LGDL fabrication

Etchant	Etch Rate (μm/min)
BOE	0.125
1% HF	1
5% HF	2

The BOE has up to this point been unable to etch through both the 25 μm and 10 μm titanium foils. An etching depth of 8 μm has been achieved after over one hour of etching. Due to this prolonged etch time, the photoresist peels off, and the desired pattern is lost. From the procedure employed in lab, the photoresist has a maximum etch time of 15 minutes before peeling off of the titanium foil. Figure 21 shows a sample of titanium foil that was etched in BOE for 60 minutes. 1% and 5% HF have both shown much higher etch rates, albeit 5% HF is more difficult to control, and etches rapidly. While both etch through the titanium foil, the 5% HF causes photoresist peel off sooner, and thus etches much of the foil surface as well. In addition, differences in the crystal structure of the foils has led to variation in the coarseness of the etched films. Figure 22 below shows preliminary etching of the both films using both 1% and 5% HF. As can be seen in the figure, the in-plane etching for the 25 μm foil is severe, and causes individual pores to etch together into one larger pore. This is due to the 1:1 aspect ratio of HF etching of titanium. For the initial photomask used in the investigation of the etchants, the spacing between mask features is about 50 μm. This has led to etched pores overlapping, as etching through the foil 25 μm leads to a pore

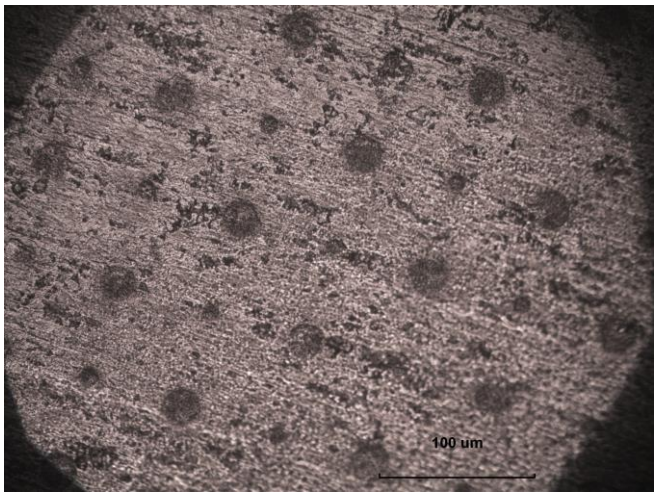

Figure 21: Titanium foil etched using BOE

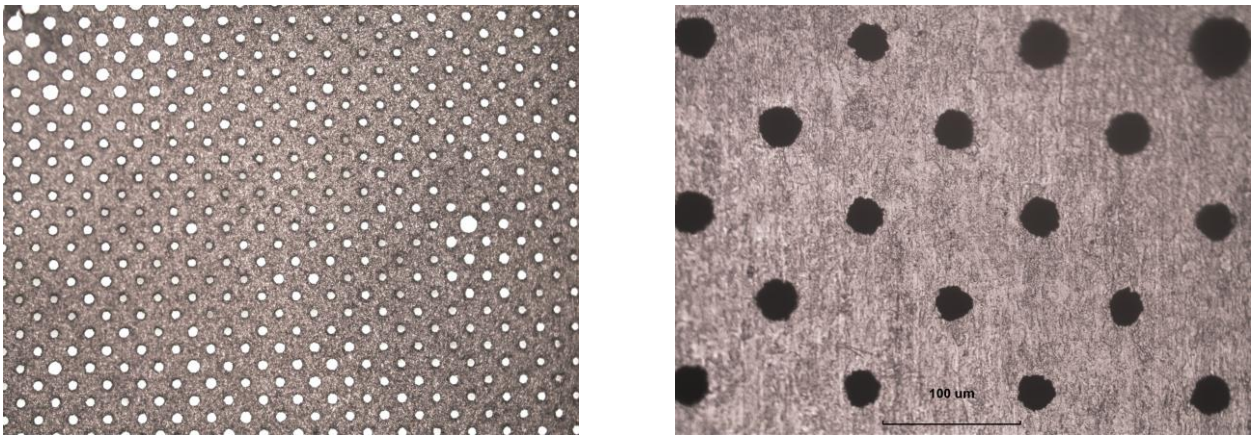

Figure 22: Etch through of titanium foil using HF (left*:* Etched pore array; right*:* Surface post etch)

radius of 25 μm. While such phenomena was expected, the ability to control and create a continuous etched surface has proved difficult. As of now a 2.5 cm^2 area of foil has been etched.

Finally, research on the use of a mixture of HF and HNO_3 as the etchant was initiated. Use of HNO_3 helps for process control during the etching of titanium, and leads to a smoother surface of the titanium post etching [45]. Figure 23 below shows the difference in the sidewalls from etching with HNO_3 added to the base HF etchant.

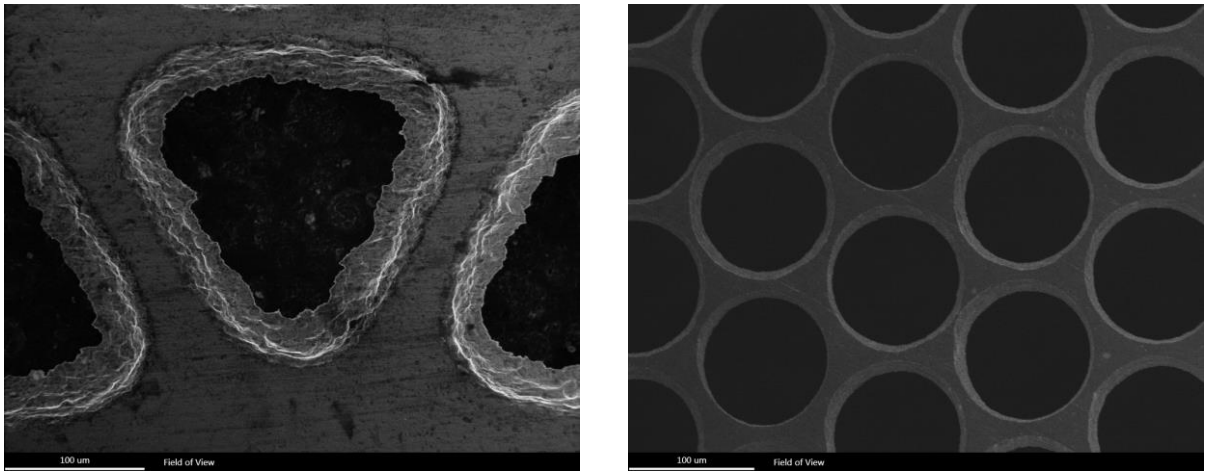

Figure 23: Sidewalls etching profile (left: HF only; right: Use of HNO_3)

CHAPTER V
CONCLUSIONS AND RECOMMENDATIONS

From the testing conducted, EDS allows for the *in-situ* investigation of the effects of porosity and thickness of the anode LGDL on the performance and efficiency of a PEMEC. In addition, GEIS has been demonstrated to characterize the interfacial contact between the LGDL and the CCM. SEM and EDS, when used together, characterize the effects of oxidation on LGDLs, and provide powerful tools to verify the diffusion of iron oxide through the membrane.

5.1 Optimal LGDL Parameters

A lack of stability in the electropotential performance of a cell indicates a high level of oxidation of the iron present in stainless steel, which is verified with the SEM and EDS characterizations. Additionally, results from the SEM and EDS analysis characterize the physical effects of oxidation on the LGDL.

Understanding the corrosion mechanism that occurs in the MEA is crucial. It has also been seen in past research that metallic cations, especially iron cations, contaminated the membrane in a PEMFC [3-5].

The corrosion and interfacial effects that occur in the LGDL-catalyst interface of a PEMEC were investigated both *in-situ* and *ex-situ* with different LGDLs. A stark difference between the SS316 mesh and the titanium mesh performance and impedance was demonstrated. A lack of stability in the electropotential performance of a cell indicates a high level of oxidation of the iron present in stainless steel, which is verified with the SEM and EDS characterizations. Additionally, results from the SEM and EDS analysis characterize the physical effects of oxidation on the LGDL.

Seven titanium gas diffusion layers, including both titanium meshes and felt, were designed to investigate the effects of LGDL porosity and thickness on the performance and impedance of a PEMEC based on the successful development of titanium bipolar plates. Both electropotential performance and galvanostatic impedance spectroscopy were conducted on the different LGDLs in order for better understanding the relations of the over potentials, ohmic resistances, and mass transport resistances.

The experiment demonstrated that the thickness and interfacial contact area of the anode LGDL with CCM play significant roles in the efficiency of a PEMEC. The performance improves with a decrease in the thickness of the anode GDL, which results in the reduction of both ohmic and transport resistances. With same thickness, the increasing of the contact area between the anode LGDL and the anode catalyst enhances the PEMEC performance due to smaller ohmic resistances. The porosity of the anode LGDL of titanium meshes does not affect the performance of PEMECs as much as in PEMFC, which usually require a porosity of 70-80% for optimal performance. The ohmic resistance plays a dominant role in electrolyzer performance, and better performance can be obtained by reducing ohmic resistance even at a lower porosity. At the investigated porosity range from 0.27 to 0.77, thin titanium LGDLs with straight pores and optimal pore sizes/porosities will be recommended for future LGDL development to minimize the ohmic loss and promote performance in PEMECs.

5.2 Recommendations

From the results, it can be very useful to develop modeling and to validate simulations of electrolyzers with optimal and repeatable performance.

An increase in understanding of the microfabrication of titanium and advances in multifunctional materials may lead to exciting advancements in associated engineering disciplines. As the field of MEMS becomes more interdisciplinary and the need for micromachinery grows, the microfabrication of titanium and other metals will become increasingly prevalent. The knowledge and processes that are expected to be developed during this research may be applied to an array of fields, from mobile technology, to aerospace structures such as nano satellite systems, and medical implants, as titanium is highly desired for its inert properties in biological systems.

The exact diffusion mechanism of iron cations through the Nafion membrane should be explored.

Thin titanium LGDLs with straight pores and optimal pore morphologies are recommended for future developments of low-cost LGDLs with minimum ohmic/transport losses.

LIST OF REFERENCES

[1] K. E. Ayers, L. T. Dalton, and E. B. Anderson, “Efficient Generation of High Energy Density Fuel from Water,” pp. 27-38, 2012.
[2] A. Marshall, B. Børresen, G. Hagen *et al.*, “Hydrogen production by advanced proton exchange membrane (PEM) water electrolysers—Reduced energy consumption by improved electrocatalysis,” *Energy,* vol. 32, no. 4, pp. 431-436, 2007.
[3] S. Grigoriev, V. Porembsky, and V. Fateev, “Pure hydrogen production by PEM electrolysis for hydrogen energy,” *International Journal of Hydrogen Energy,* vol. 31, no. 2, pp. 171-175, 2006.
[4] S. Park, J.-W. Lee, and B. N. Popov, “Effect of carbon loading in microporous layer on PEM fuel cell performance,” *Journal of Power Sources,* vol. 163, no. 1, pp. 357-363, 2006.
[5] K. Eom, E. Cho, J. Jang *et al.*, “Optimization of GDLs for high-performance PEMFC employing stainless steel bipolar plates,” *International Journal of Hydrogen Energy,* vol. 38, no. 14, pp. 6249-6260, 2013.
[6] M. Prasanna, H. Y. Ha, E. A. Cho *et al.*, “Influence of cathode gas diffusion media on the performance of the PEMFCs,” *Journal of Power Sources,* vol. 131, no. 1-2, pp. 147-154, 2004.
[7] F.-Y. Zhang, A. K. Prasad, and S. G. Advani, “Investigation of a copper etching technique to fabricate metallic gas diffusion media,” *Journal of Micromechanics and Microengineering,* vol. 16, no. 11, pp. N23-N27, 2006.
[8] E. C. Kumbur, K. V. Sharp, and M. M. Mench, “On the effectiveness of Leverett approach for describing the water transport in fuel cell diffusion media,” *Journal of Power Sources,* vol. 168, no. 2, pp. 356-368, 2007.
[9] Y. Wang, K. S. Chen, J. Mishler *et al.*, “A review of polymer electrolyte membrane fuel cells: technology, applications, and needs on fundamental research,” *Applied Energy,* vol. 88, no. 4, pp. 981-1007, 2011.
[10] P. M. Wilde, M. Maendle, M. Murata *et al.*, “Structural and physical properties of GDL and GDL/BPP combinations and their influence on PEMFC performance,” *Fuel Cells,* vol. 4, no. 3, pp. 180-184, 2004.
[11] F. Zhang, X. Yang, and C. Wang, “Liquid water removal from a polymer electrolyte fuel cell,” *Journal of the Electrochemical Society,* vol. 153, no. 2, pp. A225-A232, 2006.
[12] F.-Y. Zhang, S. G. Advani, and A. K. Prasad, “Performance of a metallic gas diffusion layer for PEM fuel cells,” *Journal of power sources,* vol. 176, no. 1, pp. 293-298, 2008.
[13] S. Park, J.-W. Lee, and B. N. Popov, “A review of gas diffusion layer in PEM fuel cells: materials and designs,” *International Journal of Hydrogen Energy,* vol. 37, no. 7, pp. 5850-5865, 2012.
[14] M. M. Mench, "Fuel Cell Engines," John Wiley & Sons, 2008.
[15] H.-Y. Jung, S.-Y. Huang, and B. N. Popov, “High-durability titanium bipolar plate modified by electrochemical deposition of platinum for unitized regenerative fuel cell (URFC),” *Journal of Power Sources,* vol. 195, no. 7, pp. 1950-1956, 2010.
[16] J. Fall, D. Humphreys, and S. Guo, “Design and testing of a unitized regenerative fuel cell,” *Journal of fuel cell science and technology,* vol. 6, no. 3, pp. 031003, 2009.

[17] G. Chen, C. C. Waraksa, H. Cho *et al.*, "EIS Studies of Porous Oxygen Electrodes with Discrete Particles I. Impedance of Oxide Catalyst Supports," *Journal of The Electrochemical Society*, vol. 150, no. 9, pp. E423-E428, 2003.
[18] H.-S. Chu, C. Yeh, and F. Chen, "Effects of porosity change of gas diffuser on performance of proton exchange membrane fuel cell," *Journal of Power Sources,* vol. 123, no. 1, pp. 1-9, 2003.
[19] M. P. Manahan, M. C. Hatzell, E. C. Kumbur *et al.*, "Laser perforated fuel cell diffusion media. Part I: Related changes in performance and water content," *Journal of Power Sources*, vol. 196, no. 13, pp. 5573-5582, 2011.
[20] S. Vengatesan, H. J. Kim, E. A. Cho *et al.*, "Operation of a proton-exchange membrane fuel cell under non-humidified conditions using thin cast Nafion membranes with different gas-diffusion media," *Journal of Power Sources,* vol. 156, no. 2, pp. 294-299, 2006.
[21] H. Ito, T. Maeda, A. Nakano *et al.*, "Influence of pore structural properties of current collectors on the performance of proton exchange membrane electrolyzer," *Electrochimica Acta,* vol. 100, pp. 242-248, 2013.
[22] G.-G. Park, Y.-J. Sohn, T.-H. Yang *et al.*, "Effect of PTFE contents in the gas diffusion media on the performance of PEMFC," *Journal of Power Sources,* vol. 131, no. 1-2, pp. 182-187, 2004.
[23] T. V. Reshetenko, G. Bender, K. Bethune *et al.*, "Effects of local variations of the gas diffusion layer properties on PEMFC performance using a segmented cell system," *Electrochimica Acta,* vol. 80, pp. 368-376, 2012.
[24] H.-C. Hsu, S.-K. Hsu, S.-C. Wu *et al.*, "Design and characterization of highly porous titanium foams with bioactive surface sintering in air," *Journal of Alloys and Compounds,* vol. 575, pp. 326-332, 2013.
[25] O. Smorygo, A. Marukovich, V. Mikutski *et al.*, "High-porosity titanium foams by powder coated space holder compaction method," *Materials Letters,* vol. 83, pp. 17-19, 2012.
[26] K. Fushinobu, D. Takahashi, and K. Okazaki, "Micromachined metallic thin films for the gas diffusion layer of PEFCs," *Journal of Power Sources,* vol. 158, no. 2, pp. 1240-1245, 2006.
[27] C.-H. Hung, C.-H. Chiu, S.-P. Wang *et al.*, "Ultra thin gas diffusion layer development for PEMFC," *International Journal of Hydrogen Energy,* vol. 37, no. 17, pp. 12805-12812, 2012.
[28] G. Lin, and T. V. Nguyen, "Effect of Thickness and Hydrophobic Polymer Content of the Gas Diffusion Layer on Electrode Flooding Level in a PEMFC," *Journal of The Electrochemical Society,* vol. 152, no. 10, pp. A1942, 2005.
[29] P. F. Chauvy, P. Hoffmann, and D. Landolt, "Applications of laser lithography on oxide film to titanium micromachining," *Applied Surface Science,* vol. 208-209, pp. 165-170, 2003.
[30] M. Bu, T. Melvin, G. J. Ensell *et al.*, "A new masking technology for deep glass etching and its microfluidic application," *Sensors and Actuators A: Physical,* vol. 115, no. 2-3, pp. 476-482, 2004.

[31] X. Lu, and Y. Leng, “Electrochemical micromachining of titanium surfaces for biomedical applications,” *Journal of Materials Processing Technology,* vol. 169, no. 2, pp. 173-178, 2005.
[32] D. Bien, P. Rainey, S. Mitchell *et al.*, “Characterization of masking materials for deep glass micromachining,” *Journal of Micromechanics and Microengineering,* vol. 13, no. 4, pp. S34, 2003.
[33] C. Iliescu, B. Chen, and J. Miao, “On the wet etching of Pyrex glass,” *Sensors and Actuators A: Physical,* vol. 143, no. 1, pp. 154-161, 2008.
[34] C. Iliescu, J. Jing, F. E. H. Tay *et al.*, “Characterization of masking layers for deep wet etching of glass in an improved HF/HCl solution,” *Surface and Coatings Technology,* vol. 198, no. 1-3, pp. 314-318, 2005.
[35] C. Iliescu, F. E. H. Tay, and J. Miao, “Strategies in deep wet etching of Pyrex glass,” *Sensors and Actuators A: Physical,* vol. 133, no. 2, pp. 395-400, 2007.
[36] M. Domanski, R. Luttge, E. Lamers *et al.*, “Submicron-patterning of bulk titanium by nanoimprint lithography and reactive ion etching,” *Nanotechnology,* vol. 23, no. 6, pp. 065306, Feb 17, 2012.
[37] M. F. Aimi, M. P. Rao, N. C. MacDonald *et al.*, “High-aspect-ratio bulk micromachining of titanium,” *Nat Mater,* vol. 3, no. 2, pp. 103-5, Feb, 2004.
[38] E. R. Parker, B. J. Thibeault, M. F. Aimi *et al.*, “Inductively Coupled Plasma Etching of Bulk Titanium for MEMS Applications,” *Journal of The Electrochemical Society,* vol. 152, no. 10, pp. C675, 2005.
[39] T. Tillocher, P. Lefaucheux, B. Boutaud *et al.*, “Alternated process for the deep etching of titanium,” *Journal of Micromechanics and Microengineering,* vol. 24, no. 7, pp. 075021, 2014.
[40] Y. Zhang, N. Li, B. Yan *et al.*, “Fabrication of laterally driven bulk titanium devices on titanium-on-glass wafers,” *Journal of Micromechanics and Microengineering,* vol. 23, no. 7, pp. 075026, 2013.
[41] G. Zhao, Q. Shu, T. Yao *et al.*, “Wafer level bulk titanium ICP etching using SU8 as an etching mask,” *Journal of Micromechanics and Microengineering,* vol. 19, no. 9, pp. 095006, 2009.
[42] Y. Wang, “Modeling of two-phase transport in the diffusion media of polymer electrolyte fuel cells,” *Journal of Power Sources,* vol. 185, no. 1, pp. 261-271, 2008.
[43] I. Zenyuk, E. Kumbur, and S. Litster, “Deterministic contact mechanics model applied to electrode interfaces in polymer electrolyte fuel cells and interfacial water accumulation,” *Journal of Power Sources,* vol. 241, pp. 379-387, 2013.
[44] A. Kalidindi, R. Taspinar, S. Litster *et al.*, “A two-phase model for studying the role of microporous layer and catalyst layer interface on polymer electrolyte fuel cell performance,” *international journal of hydrogen energy,* vol. 38, no. 22, pp. 9297-9309, 2013.
[45] Kulkarni, Milind S., and Henry F. Erk. "Acid-Based Etching of Silicon Wafers: Mass-Transfer and Kinetic Effects." *Journal of The Electrochemical Society* 147, no. 1 (2000): 176-188.

VITA

Stuart McCoy Steen III was born and raised in Fairfax, Virginia. After graduating from Robinson Secondary School with an International Baccalaureate Diploma in 2009, he entered the University of Virginia in Charlottesville, Virginia. He received his Bachelors of Science in Aerospace Engineering with a minor in Applied Mathematics from UVa in the spring of 2013. After graduation, Stuart accepted a graduate research assistantship at the University of Tennessee Space Institute (UTSI) working for Dr. Feng Yuan Zhang. He recently completed an internship at Naval Research Laboratory where he worked in the Thermal Systems & Analysis Branch of the Spacecraft Technology Division. Stuart currently resides in Murfreesboro, Tennessee along with his girlfriend and their cat.